Hybrid Nanoparticles

DOI: 10.1002/anie.201007794

Plasmonic/Magnetic Bifunctional Nanoparticles**

*Sheng Peng, Changhui Lei, Yang Ren, Russell E. Cook, and Yugang Sun**

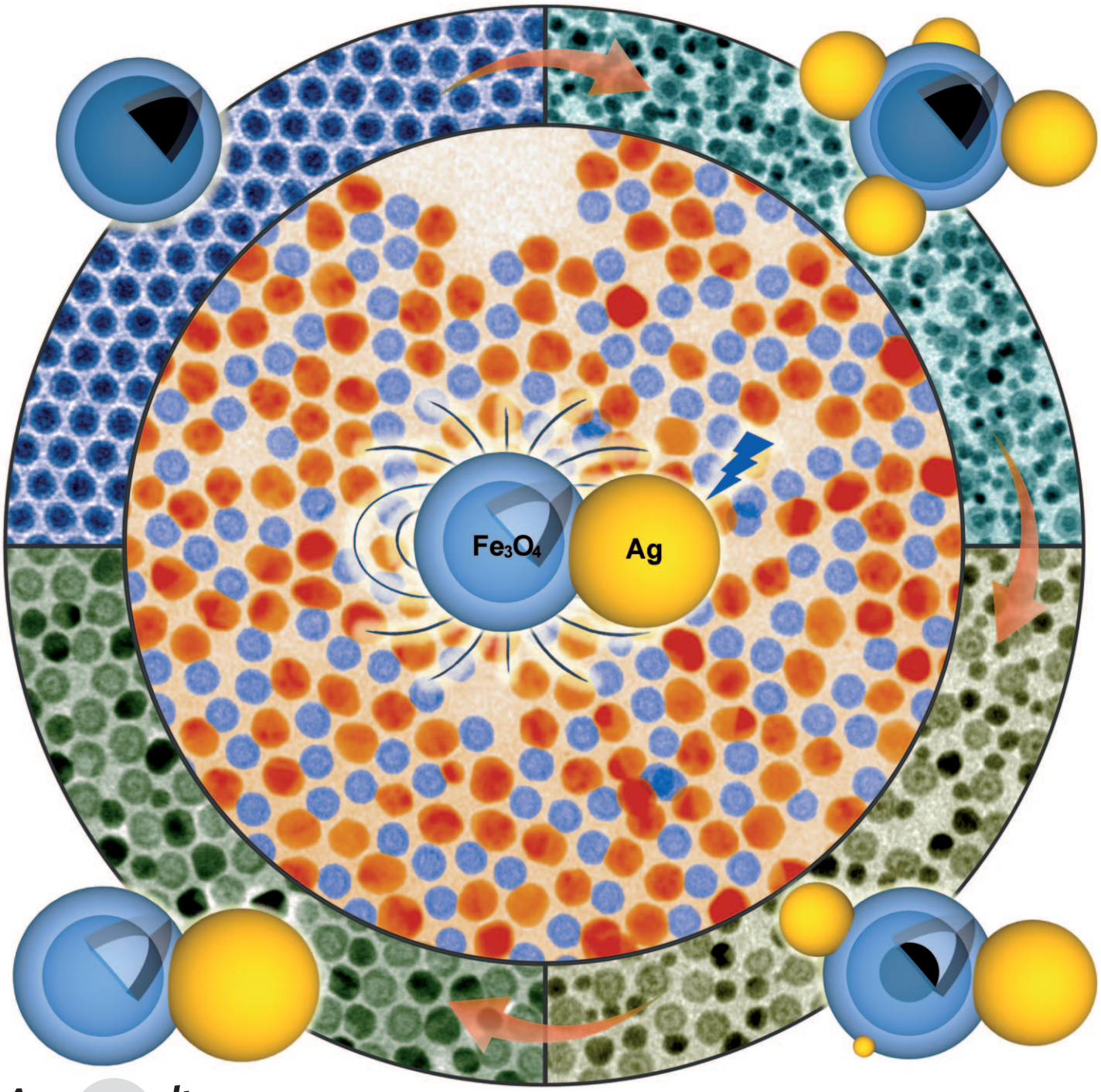

Hybrid nanoparticles composed of multiple components usually exhibit multiple functionalities. These nanoparticles attract tremendous research interest because of their unique properties and applications that are difficult (or even impossible) to achieve from single-component nanoparticles.[1–6] For example, hybrid magnetic/metallic nanoparticles represent an important class of nanomaterials because of applications in, for example, recoverable catalysis,[7] drug delivery,[8] multimodal imaging, and therapy in biomedicine.[9] As a result, the development of facile strategies for the synthesis of such hybrid nanoparticles is very intriguing. Sun and co-workers have developed a seed-mediated approach where metal nanoparticles (e.g., Au and Pt) are used as seeds and the Fe_3O_4 component is epitaxially deposited on the surfaces of the metal nanoparticles by decomposition of $Fe(CO)_5$ followed by oxidation in an appropriate solvent (e.g., 1-octadecene).[2a] The resulting hybrid nanoparticles exhibit a dumbbell-like morphology, and the sizes of the metal nanoparticles are much smaller than that of the Fe_3O_4 nanoparticles. Further enlargement of the metal nanoparticles usually leads to their detachment from the Fe_3O_4 particles because of the increased mechanical stress.[10] An alternative strategy relies on the modification of Fe_3O_4 nanoparticles with an amorphous layer (e.g., a biological bilayer[11] or SiO_2[12]) that can mediate the deposition of Au to form magnetic/metal core/shell nanoparticles. Incorporation of the amorphous layers can help avoid the mechanical stress caused by lattice mismatch in the hybrid nanoparticles, thus resulting in the possibility to tune the lateral dimensions of the Au nanoshells over a wide range. Herein, we report a facile strategy that uses Fe nanoparticles coated with a thin layer of amorphous iron oxide (abbreviated as Fe_xO_y regardless of the exact composition), which is spontaneously formed during the post-synthesis washing, as seeds for the direct nucleation and growth of Ag nanodomains on the nanoparticle surfaces. The number and size of the Ag domains in each hybrid particle can be tuned by controlling the reaction time and the concentration of the precursor (i.e., $AgNO_3$).

Figure 1 shows the major steps involved in the seed-mediated synthesis of Ag–Fe_xO_y hybrid nanoparticles that exhibit both plasmonic and magnetic properties. In a typical

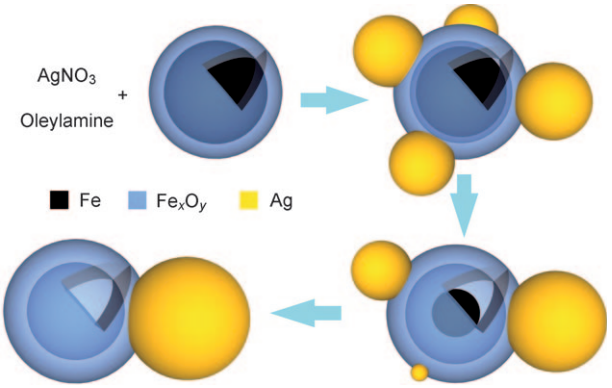

Figure 1. The major steps involved in the synthesis of plasmonic/magnetic bifunctional nanoparticles by chemical reduction of $AgNO_3$ with oleylamine at high temperature in the presence of Fe/Fe_xO_y core/shell nanoparticles as seeds.

synthesis, monodispersed Fe nanoparticles with uniform sizes (e.g., 5–15 nm) are first synthesized through thermal decomposition of $Fe(CO)_5$ in 1-octadecene (ODE) containing oleylamine (OAm; see the Supporting Information).[13] For example, heating 0.30 mL of $Fe(CO)_5$ in 10 mL of ODE (with 0.30 mL of OAm) under an N_2 atmosphere at 180 °C for 20 min generates nanoparticles with diameters of approximately 14 nm (standard size deviation $<7\%$), which are strongly attached to the magnetic stir bar. The stir bar is then washed with hexane to release the nanoparticles, thus indicating that the magnetic moment of the nanoparticles significantly decreases. The change of magnetic properties is ascribed to the surface oxidation of the Fe nanoparticles into iron oxides that exhibit much a smaller magnetic moment than pure iron. As a result, core/shell nanoparticles consisting of Fe cores with a diameter of approximately 9 nm and amorphous Fe_xO_y shells with a thickness of approximately 2.5 nm are formed by partial oxidation of the iron nanoparticles with the trace oxygen dissolved in the hexane (Figure S1a,b). Formation of the thin Fe_xO_y shells can passivate the nanoparticles and significantly prevent the inner Fe cores from quick oxidation.[14] The X-ray diffraction (XRD) pattern of the as-synthesized Fe/Fe_xO_y core/shell nanoparticles exhibits very broad peaks (Figure S1c), thus indicating that both the Fe cores and oxide shells are amorphous. In the second step, injection of a solution of $AgNO_3$ in OAm to a hot dispersion of the amorphous Fe/Fe_xO_y nanoparticles in a mixture of ODE and OAm leads to decoration of the magnetic nanoparticles with Ag nanodomains: once the $AgNO_3$ is in contact with the hot solvent, OAm molecules instantaneously reduce Ag^+ ions to Ag atoms that will condense on the surfaces of the Fe/Fe_xO_y nanoparticles to form Ag nanodomains. The amorphous

[*] Dr. S. Peng, Dr. Y. Sun
Center for Nanoscale Materials, Argonne National Laboratory
9700 South Cass Avenue, Argonne, IL 60439 (USA)
E-mail: ygsun@anl.gov
Dr. Y. Ren
X-Ray Science Division, Advanced Photon Source
Argonne National Laboratory, Argonne, IL 60439 (USA)
Dr. R. E. Cook
Electron Microscopy Center, Materials Science Division, Argonne National Laboratory, Argonne, IL 60439 (USA)
Dr. C. Lei
Center for Microanalysis of Materials
Frederick Seitz Materials Research Laboratory
University of Illinois at Urbana-Champaign, Urbana, IL 61801 (USA)

[**] Use of the Center for Nanoscale Materials, Advanced Photon Source (11ID-C), and Electron Microscopy Center for Materials Research at Argonne National Laboratory was supported by the U.S. Department of Energy, Office of Science, Office of Basic Energy Sciences, under contract no. DE-AC02-06CH11357. Use of the Center for Microanalysis of Materials Facilities in Frederick Seitz Materials Research Laboratory, University of Illinois, is partially supported by the U.S. Department of Energy under grants DE-FG02-07ER46453 and DE-FG02-07ER46471.

Supporting information for this article is available on the WWW under http://dx.doi.org/10.1002/anie.201007794.

Fe_xO_y shells provide the nucleation sites for the growth of Ag domains because of the low interfacial energy between the amorphous Fe_xO_y and crystalline Ag. The synergy between the fast reduction of Ag^+ ions and heterogeneous nucleation leads to the formation of multiple Ag domains (as many as eight) on the surface of each Fe/Fe_xO_y seed nanoparticle. Continuous heating of the reaction system initiates the ripening process of the Ag domains, thus resulting in a gradual decrease in the average number (n_d) of the Ag domains on each magnetic Fe/Fe_xO_y nanoparticle. During the ripening process, the larger Ag domains are continuously enlarged as the smaller domains are consumed, and the Fe cores are converted to hollow Fe_xO_y nanoparticles by oxidation. When the ripening time is sufficiently long, dumbbell-like nanoparticles are formed and each particle consists of a hollow Fe_xO_y nanoshell and a solid Ag domain. It is noteworthy that the ripening process neither destructs the interface between the Fe_xO_y and Ag nor detaches the Ag domains from the magnetic ones. The interfacial stability between the Fe_xO_y and Ag domains benefits from the consistent amorphous nature of the Fe_xO_y shells during the entire reaction. The number and size of the Ag domains in the hybrid nanoparticles can be easily tuned by controlling the reaction time and the concentration of $AgNO_3$.

Figure 2 shows a series of typical TEM images of the samples obtained by injecting a solution of $AgNO_3$ in OAm (0.05 M, 2.0 mL) into hot ODE (10 mL, 180 °C) containing OAm (0.5 mL) and Fe/Fe_xO_y core/shell nanoparticles (12 mg; Figure S1) that serve as seeds, followed by continuous heating for different times. The Fe/Fe_xO_y seed nanoparticles maintain their size and morphology after they are heated in the hot ODE (with OAm) at 180 °C under an N_2 atmosphere (compare Figure 2a and Figure S1a). Once the $AgNO_3$ solution is injected, an intense yellow color instantaneously appears within 1 s in the reaction mixture, thus indicating the formation of Ag nanoparticles that exhibit a strong optical absorption in blue region of the spectrum because of their surface plasmon resonance (SPR).[15] TEM studies reveal that multiple particulate nanodomains of Ag are grown on the surface of each Fe/Fe_xO_y nanoparticle for the samples formed at the beginning of the reaction, for example, at 2 s (Figure 2b). Statistical analysis over a large number of particles observed in the TEM images (Figure S2) gives an average of 3.6 Ag domains in each hybrid particle (i.e., $n_d = 3.6$; Figure S3a,i). The number of Ag domains can be as high as eight and the inset of Figure 2b shows a particle that contains seven Ag domains. The number of Ag domains of most particles is reduced to two or three when the reaction proceeds to 30 s (Figure 2c). The average number of Ag domains in each particle continues to decrease as the reaction time is extended (e.g., $n_d = 1.48$ at 90 s for the sample shown in Figure 2d, and 1.25 at 180 s for the sample shown in Figure 2e; Figure S3). When the reaction time is sufficiently long, for example, 300 s, the product is dominated by dumbbell-like dimers (ca. 75%), each of which consists of a single Ag domain and a hollow Fe_xO_y shell (Figure 2f). In addition, the dimensions of the Ag domains and the morphology of the Fe/Fe_xO_y seed nanoparticles also undergo significant changes in the course of the reaction. For example, the Ag domains exhibit a similar size

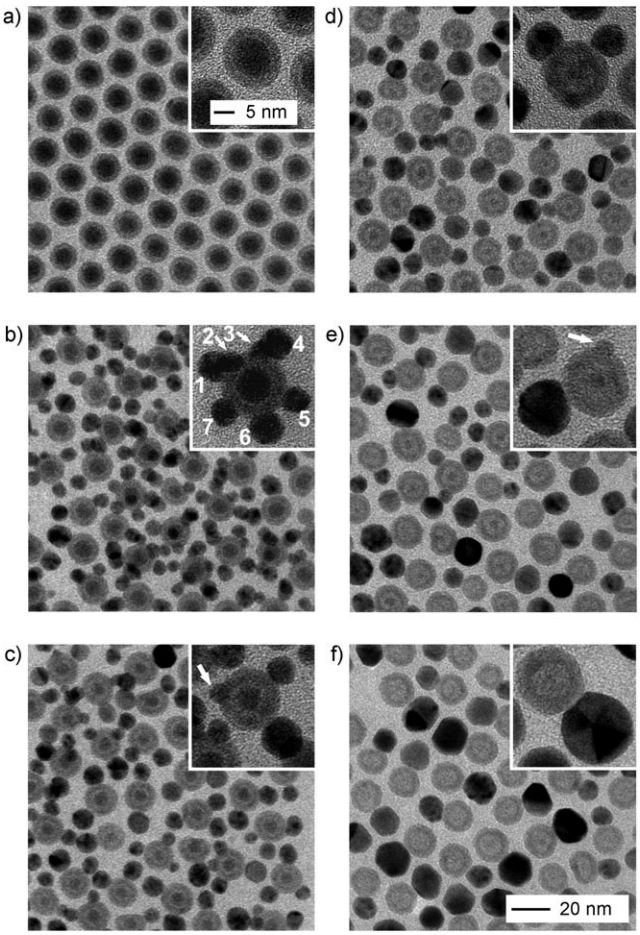

Figure 2. TEM images of nanoparticles obtained at different reaction times (normalized against the time when the $AgNO_3$ solution was injected to the dispersion of Fe/Fe_xO_y seed nanoparticles): a) 0, b) 2, c) 30, d) 90, e) 180, and f) 300 s. The insets highlight the representative individual particles. The numbers and arrows in the inset of frame (b) highlight a hybrid particle containing seven Ag domains. The arrows in the insets of frames (c) and (e) highlight two "dissolving" Ag domains. The scale bar in (f) applies to all images, and the scale bar in the inset of frame (a) also applies to all insets.

(i.e., ca. 7 nm in diameter) in the sample formed at 2 s because of the fast nucleation and growth of Ag on the amorphous Fe_xO_y shells. As the reaction proceeds, the Ag domains on an individual particle differentiate in a way that the most stable Ag domain continuously grows larger while the others gradually shrink and eventually disappear (see Figure 2c–e). The variations in the number and size of the Ag domains as a function of the reaction time are consistent with the classical LaMer nucleation and Ostwald ripening processes, in which the growth of nanoparticles is initiated from a single-step, fast nucleation event followed by subsequent growth of the larger, more stable particles with the consumption of the smaller particles by diffusion of solute species.[16] For the sample dominated by the dumbbell-like dimers (Figure 2f), the size of the Ag domains reaches approximately 15 nm. Meanwhile, the Fe cores of the Fe/Fe_xO_y seed nanoparticles gradually shrink (e.g., ca. 8 nm at 2 s versus ca. 4 nm at 90 s) and disappear when the reaction time

is long enough (e.g., 300 s), to result in the formation of Fe_xO_y shells with hollow interiors and thicker walls in comparison with the Fe_xO_y shells in the original seed particles. This kind of morphological evolution associated with chemical transformation is consistent with the oxidative Kirkendall diffusions reported elsewhere that are responsible for the formation of hollow nanoparticles.[17] Oxidation of the Fe nanoparticles is ascribed to the oxidizing ability of nitrate ions at elevated temperatures, and possible trace amounts of dissolved oxygen in the precursor solution of $AgNO_3$, and Ag^+ ions (Figure S4).[18] The evolution of the Ag domains in terms of the size and number is consistent with the variation of UV/Vis absorption spectra measured at different reaction times (Figure S5).[15,19]

Once the dumbbell-like particles are formed, further increases in the ripening time cannot significantly change their morphology while the population of dimers slightly increases (for example, ca. 80% for the sample formed at 600 s versus ca. 75% for the sample formed at 300 s; compare Figure S6 with Figure 2 f). As shown in Figure 3, the dumbbell

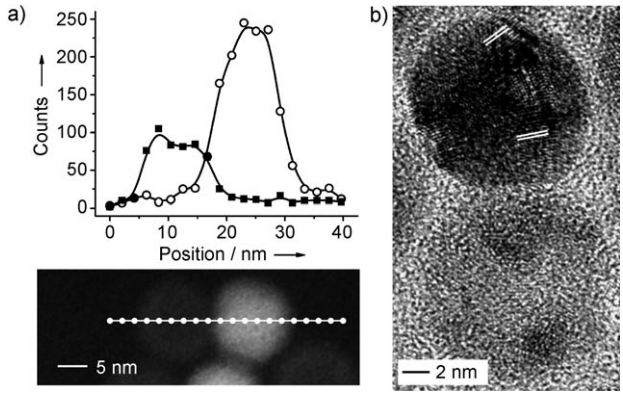

Figure 3. Characterization of Ag–Fe_xO_y dumbbell-like nanoparticles formed at 600 s with a) high-resolution line-scan EDS analysis of Ag (○) and Fe (■), and b) HRTEM. The line and dots in the high-angle annular dark-field scanning transmission electron microscopy (HAADF-STEM) image (bottom frame in (a)) show the scanning path and the corresponding examining positions. The adjacent lattice fringes in (b) are measured to be 0.238 nm that matches well with the (111) interplanar distance of fcc Ag.

particle consists of a 17 nm solid Ag domain and a 17 nm hollow Fe_xO_y shell. High-resolution line-scan energy dispersive X-ray spectroscopy (EDS) shows a sharp differentiation of Fe and Ag along the scanning path across both the Fe_xO_y shell and the Ag domain in a dimer particle (Figure 3 a), thus indicating that the interdiffusion between iron oxide and Ag is negligible under the current reaction conditions. High-resolution TEM (HRTEM) images (Figure 3 b) of individual dumbbell particles reveal the high crystallinity of the Ag domains and the amorphous (or very low) crystallinity of the hollow Fe_xO_y shells as well as the clear interface between Fe_xO_y and Ag. The XRD pattern of the same sample exhibits only diffraction peaks that originate from Ag with a face-centered cubic (fcc) phase (Figure S7c). The absence of the feature peaks associated with iron oxides (e.g., FeO, Fe_3O_4, and Fe_2O_3) further confirms the amorphous character of the Fe_xO_y shells. A systematic HRTEM study proves that the amorphous character of the Fe_xO_y shells is inherited along the entire reaction for the formation of dumbbell nanoparticles from the Fe/Fe_xO_y seeds (Figure S8). These results indicate that the amorphous character associated with the Fe_xO_y shells may play an important role in facilitating the formation of hybrid nanoparticles. In a control synthesis, the Fe/Fe_xO_y seed nanoparticles (Figure S1) are first oxidized by bubbling with air at 180 °C followed by mixing with a solution of $AgNO_3$ (see the Supporting Information for detailed procedures). The seeds become polycrystalline Fe_3O_4 nanoshells with hollow interiors (Figure S7b, S9e and inset).[17] The increased crystallinity of the seeds drastically changes the kinetics of the reduction of the Ag^+ ions and growth of the Ag domains. Upon injection of the solution of $AgNO_3$ to the dispersion of Fe_3O_4 seeds, the Ag^+ ions are reduced slower than in the typical synthesis in the presence of the amorphous seeds (Figure 2 a), where the Ag^+ ions are essentially reduced completely within a very short period (Figure S10). As a result, short reaction times (i.e., 2 s) lead to the deposition of only one small Ag domain (with size of ca. 2 nm) on each Fe_3O_4 shell (Figure S9 f). As the reaction proceeds, the Ag domains increase in size (e.g., ca. 8 nm at 120 s), while the number of the Ag domains on the Fe_3O_4 seed shells remains unchanged. Meanwhile, many free Ag nanoparticles with small sizes (ca. 4 nm) are formed in solution through self-nucleation and growth (Figure S9 g). Continuous growth of the Ag domains adhered to the Fe_3O_4 shells forces them to detach from the Fe_3O_4 surfaces (see Figure S9 h for the sample formed at 300 s). The detachment and the deformation of the dumbbell-like dimers might be due to the increased stress at the interface as the Ag domains grow.[10] The difference between the reaction systems with different seeds (i.e., amorphous Fe/Fe_xO_y core/shell particles versus polycrystalline Fe_3O_4 nanoshells) indicates that amorphous surfaces are more suitable for the nucleation of crystalline Ag. The amorphous Fe_xO_y surfaces can provide a high density of nucleation sites than crystalline iron oxide to accelerate the reduction of Ag^+ ions and facilitate the growth of a larger number of Ag domains on the surfaces. In contrast, the reduction rate of Ag^+ ions becomes extremely slow if no seeds are presented in the reaction system. For example, no crystalline Ag nanoparticles can be formed even when the reaction lasts for 20 s (Figure S10). Similar to the synthesis of nanoparticles in homogeneous solutions, longer reaction times can result in the formation of Ag nanoparticles through self-nucleation followed by sequential growth (Figure S9a–d).

In addition to the unique optical properties associated with the plasmonic Ag domains (Figure S5a), the hybrid nanoparticles shown in Figure 2 b–f and Figure 3 also exhibit superparamagnetic properties at room temperature because of the existence of Fe/Fe_xO_y core/shell particles or Fe_xO_y hollow shells. Magnetic hysteresis loops of different hybrid nanoparticles at room temperature are compared in Figure 4. The nanoparticles formed at 2 s (Figure 2 b) have a saturation moment of approximately 12 emu g^{-1} (Figure 4, curve a) that accounts for a decrease of more than 80% compared to the value of the original Fe/Fe_xO_y seed nanoparticles

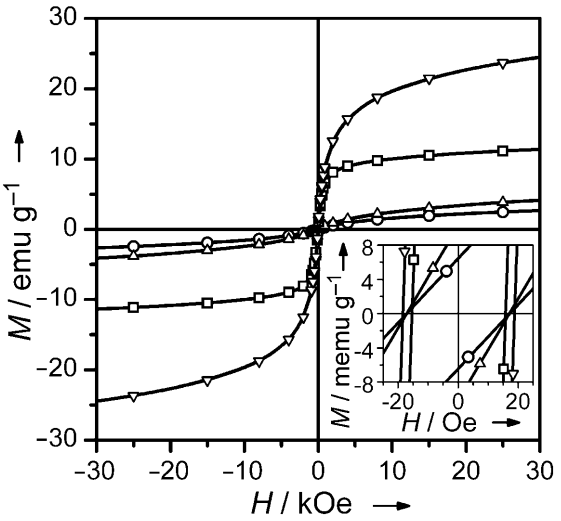

Figure 4. Room-temperature magnetic hysteresis loops of a) hybrid nanoparticles with multiple Ag domains as shown in Figure 2b (□); b) dumbbell-like hybrid particles as shown in Figure 3 (○); c) particles in (b) oxidized by bubbling with air at 180 °C for 20 min (△); and d) particles in (b) oxidized with Me_3NO at 180 °C for 20 min (▽). The inset shows an enlarged area close to the origin.

(ca. 67 emu g^{-1} for the particles shown in Figure S1).[13] This decrease in magnetic moment is ascribed to the incorporation of massive diamagnetic Ag that dilutes the magnetic response of the Fe/Fe_xO_y components. Although the Fe_xO_y shells can somehow protect the inside Fe cores, the nanoparticles are still not stable when they are exposed to a strong oxidative environment. As shown in Figure 3, reaction for 600 s transforms the Fe/Fe_xO_y domains to complete amorphous Fe_xO_y hollow shells. The corresponding hybrid nanoparticles exhibit a very low magnetic moment of approximately 3 emu g^{-1} (Figure 4, curve b), thus indicating that the amorphous (or low-crystalline) Fe_xO_y hollow shells that contain small grains may be subject to thermal agitation and surface spin-canting effects.[20] An increase in the crystallinity of the Fe_xO_y shells is therefore expected to increase the magnetic moment of the hybrid nanoparticles shown in Figure 3. Oxidation of the as-synthesized hybrid nanoparticles by flushing the reactor with air at 180 °C for 20 min can convert the amorphous Fe_xO_y shells to polycrystalline Fe_3O_4 shells with grain sizes of 3–5 nm and a magnetic moment that is slightly enhanced to approximately 5 emu g^{-1} (Figure 4, curve c). On the other hand, a more aggressive oxidization with trimethylamine *N*-oxide (Me_3NO)[17] can convert the Fe_xO_y shells into Fe_3O_4 shells with large grain sizes (5–10 nm), which lead to a significant enhancement in their magnetic moment of up to around 25 emu g^{-1} (Figure 4, curve d). It is noteworthy that the post-oxidation process does not destroy the dumbbell-like morphology of the hybrid nanoparticles (Figure S11). Regardless of their exact compositions and morphologies, the hybrid nanoparticles are superparamagnetic at room temperature with small coercivities less than 20 Oe (Figure 4, inset).

In summary, a very simple protocol, which involves the chemical reduction of Ag^+ ions in the presence of Fe nanoparticles with amorphous Fe_xO_y surfaces, has been developed for synthesizing hybrid nanoparticles that have both plasmonic and magnetic properties. At the very beginning of the reaction, the hybrid nanoparticles consist of single Fe/Fe_xO_y core/shell nanoparticles, and multiple Ag nanodomains can be formed on the nanoparticle surfaces. The superparamagnetic properties and near-field coupling behavior between different Ag domains may enable the nanoparticles to serve as substrates for surface-enhanced Raman scattering (SERS)[12] and contrast agents for magnetic resonance imaging (MRI) and optical imaging.[9a,b] Dumbbell-like nanoparticles consisting of single Fe_3O_4 hollow nanoshells and single Ag domains are formed after a sufficiently long reaction time, followed by post-oxidation. The combination of the hollow structure of the Fe_3O_4 nanoshells and the SPR of the Ag domains may make them suitable for drug delivery and therapy.[8,9b,c] The size of Ag domains in the dumbbell nanoparticles and thus their optical properties can be tuned by controlling the reaction time and the concentration of $AgNO_3$ (Figure S12). By substituting the solution of $AgNO_3$ with that of other precursors, hybrid nanoparticles consisting of iron oxide nanoshells and other metal nanodomains can also be synthesized. For instance, injection of a solution of [$Cu(acac)_2$] (acac = acetylacetonate) in OAm (0.05 M, 2.0 mL) into the dispersion of Fe/Fe_xO_y seed nanoparticles that is used for the synthesis of hybrid particles (Figure 2) leads to the formation of dimers and each consists of a 17 nm hollow Fe_xO_y nanoshell and a 17 nm Cu nanodomain (Figure S13a). The resulting Cu–Fe_xO_y hybrid particles also exhibit superparamagnetic properties and optical properties that correspond to the SPR of Cu nanoparticles, that is, an absorption peak at approximately 580 nm (Figure S13c).[21]

Received: December 10, 2010
Revised: February 1, 2011
Published online: March 4, 2011

Keywords: iron oxide · magnetic properties · nanoparticles · silver · surface plasmon resonance

[1] For reviews, see, for example: a) R. Costi, A. E. Saunders, U. Banin, *Angew. Chem.* **2010**, *122*, 4996; *Angew. Chem. Int. Ed.* **2010**, *49*, 4878; b) C. Minelli, S. B. Lowe, M. M. Stevens, *Small* **2010**, *6*, 2336; c) R. Hao, R. Xing, Z. Xu, Y. Hou, S. Gao, S. Sun, *Adv. Mater.* **2010**, *22*, 2729; d) P. Zrazhevskiy, M. Sena, X. Gao, *Chem. Soc. Rev.* **2010**, *39*, 4326; e) J. Gao, H. Gu, B. Xu, *Acc. Chem. Res.* **2009**, *42*, 1097.

[2] For metal magnetic hybrid nanoparticles, see: a) H. Yu, M. Chen, P. M. Rice, S. X. Wang, R. L. White, S. Sun, *Nano Lett.* **2005**, *5*, 379; b) H. Gu, Z. Yang, J. Gao, C. K. Chang, B. Xu, *J. Am. Chem. Soc.* **2005**, *127*, 34; c) E. V. Shevchenko, M. I. Bodnarchuk, M. V. Kovalenko, D. V. Talapin, R. K. Smith, S. Aloni, W. Heiss, A. P. Alivisatos, *Adv. Mater.* **2008**, *20*, 4323; d) F. Wetz, K. Soulantica, A. Falqui, M. Respaud, E. Snoeck, B. Chaudret, *Angew. Chem.* **2007**, *119*, 7209; *Angew. Chem. Int. Ed.* **2007**, *46*, 7079; e) D. Wang, Y. Li, *J. Am. Chem. Soc.* **2010**, *132*, 6280.

[3] For metal chalcogenide semiconductor hybrid nanoparticles, see: a) J. Zeng, J. Huang, C. Liu, C. H. Wu, Y. Lin, X. Wang, S. Zhang, J. Hou, Y. Xia, *Adv. Mater.* **2010**, *22*, 1936; b) T. Mokari, E. Rothenberg, I. Popov, R. Costi, U. Banin, *Science* **2004**, *304*, 1787; c) S. E. Habas, P. Yang, T. Mokari, *J. Am. Chem. Soc.* **2008**,

130, 3294; d) J. Zhang, Y. Tang, K. Lee, M. Ouyang, *Science* **2010**, *327*, 1634; e) M. Pang, J. Hu, H. C. Zeng, *J. Am. Chem. Soc.* **2010**, *132*, 10771.

[4] For metal oxide semiconductor hybrid nanoparticles, see: a) Y. Dai, B. Lim, Y. Yang, C. M. Cobley, W. Li, E. C. Cho, B. Grayson, P. T. Fanson, C. T. Campbell, Y. Sun, Y. Xia, *Angew. Chem.* **2010**, *122*, 8341; *Angew. Chem. Int. Ed.* **2010**, *49*, 8165; b) T. D. Schladt, M. I. Shukoor, K. Schneider, M. N. Tahir, F. Natalio, I. Ament, J. Becker, F. D. Jochum, S. Weber, O. Köhler, P. Theato, L. M. Schreiber, C. Sönnichsen, H. C. Schröder, W. E. G. Müller, W. Tremel, *Angew. Chem.* **2010**, *122*, 4068; *Angew. Chem. Int. Ed.* **2010**, *49*, 3976; c) W. H. Hung, M. Aykol, D. Valley, W. Hou, S. B. Cronin, *Nano Lett.* **2010**, *10*, 1314; d) T. Kayama, K. Yamazaki, H. Shinjoh, *J. Am. Chem. Soc.* **2010**, *132*, 13154; e) Y. Tian, T. Tatsuma, *J. Am. Chem. Soc.* **2005**, *127*, 7632.

[5] For metal halogenide semiconductor hybrid nanoparticles, see: a) P. Wang, B. Huang, X. Qin, X. Zhang, Y. Dai, J. Wei, M.-H. Whangbo, *Angew. Chem.* **2008**, *120*, 8049; *Angew. Chem. Int. Ed.* **2008**, *47*, 7931; b) C. An, S. Peng, Y. Sun, *Adv. Mater.* **2010**, *22*, 2570; c) P. Wang, B. Huang, X. Zhang, X. Qin, H. Jin, Y. Dai, Z. Wang, J. Wei, J. Zhan, S. Wang, J. Wang, M.-H. Whangbo, *Chem. Eur. J.* **2009**, *15*, 1821; d) C. Hu, T. Peng, X. Hu, Y. Nie, X. Zhou, J. Qu, H. He, *J. Am. Chem. Soc.* **2010**, *132*, 857; e) Y. Sun, *J. Phys. Chem. C* **2010**, *114*, 2127.

[6] For metal/other semiconductor hybrid nanoparticles: a) Y. Sun, *Adv. Funct. Mater.* **2010**, *20*, 3646; b) Y. Sun, G. P. Wiederrecht, *Small* **2007**, *3*, 1964; c) Y. Qu, L. Liao, R. Cheng, Y. Wang, Y.-C. Lin, Y. Huang, X. Duan, *Nano Lett.* **2010**, *10*, 1941.

[7] a) C. Wang, H. Daimon, S. Sun, *Nano Lett.* **2009**, *9*, 1493; b) C. Wang, H. Yin, S. Dai, S. Sun, *Chem. Mater.* **2010**, *22*, 3277.

[8] C. Xu, B. Wang, S. Sun, *J. Am. Chem. Soc.* **2009**, *131*, 4216.

[9] a) C. Xu, J. Xie, D. Ho, C. Wang, N. Kohler, E. G. Walsh, J. R. Morgan, Y. E. Chin, S. Sun, *Angew. Chem.* **2008**, *120*, 179; *Angew. Chem. Int. Ed.* **2008**, *47*, 173; b) J. Gao, G. Liang, J. S. Cheung, Y. Pan, Y. Kuang, F. Zhao, B. Zhang, X. Zhang, E. X. Wu, B. Xu, *J. Am. Chem. Soc.* **2008**, *130*, 11828; c) K. Cheng, S. Peng, C. Xu, S. Sun, *J. Am. Chem. Soc.* **2009**, *131*, 10637.

[10] C. Wang, Y. Wei, H. Jiang, S. Sun, *Nano Lett.* **2009**, *9*, 4544.

[11] Y. Jin, C. Jia, S.-W. Huang, M. O'Donnell, X. Gao, *Nat. Commun.* **2010**, *1*, 41.

[12] Q. Zhang, J. Ge, J. Goebl, Y. Hu, Y. Sun, Y. Yin, *Adv. Mater.* **2010**, *22*, 1905.

[13] S. Peng, C. Wang, J. Xie, S. Sun, *J. Am. Chem. Soc.* **2006**, *128*, 10676.

[14] C. M. Wang, D. R. Baer, L. E. Thomas, J. E. Amonette, J. Antony, Y. Qiang, G. Duscher, *J. Appl. Phys.* **2005**, *98*, 094308.

[15] K. L. Kelly, E. Coronado, L. L. Zhao, G. C. Schatz, *J. Phys. Chem. B* **2003**, *107*, 668.

[16] a) C. B. Murray, C. R. Kagan, M. G. Bawendi, *Annu. Rev. Mater. Sci.* **2000**, *30*, 545; b) W. Z. Ostwald, *Z. Phys. Chem.* **1901**, *37*, 385; c) I. M. Lifshitz, V. V. Slyozov, *J. Phys. Chem. Solids* **1961**, *19*, 35.

[17] S. Peng, S. Sun, *Angew. Chem.* **2007**, *119*, 4233; *Angew. Chem. Int. Ed.* **2007**, *46*, 4155.

[18] S. Peng, Y. Sun, *Chem. Mater.* **2010**, *22*, 6272.

[19] S. Peng, J. M. McMahon, G. C. Schatz, S. K. Gray, Y. Sun, *Proc. Natl. Acad. Sci. USA* **2010**, *107*, 14530.

[20] a) B. Martínez, X. Obradors, L. Balcells, A. Rouanet, C. Monty, *Phys. Rev. Lett.* **1998**, *80*, 181; b) C. Martínez-Boubeta, K. Simeonidis, M. Angelakeris, N. Pazos-Pérez, M. Giersig, A. Delimitis, L. Nalbandian, V. Alexandrakis, D. Niarchos, *Phys. Rev. B* **2006**, *74*, 054430.

[21] L.-I. Hung, C.-K. Tsung, W. Huang, P. Yang, *Adv. Mater.* **2010**, *22*, 1910.

